HMI Data Driven Magnetohydrodynamic Model Predicted Active Region Photospheric Heating Rates: Their Scale Invariant, Flare Like Power Law Distributions, and Their Possible Association With Flares

Michael L. Goodman[1], Chiman Kwan[2], Bulent Ayhan[2], and Eric L. Shang[2]

[1]Jacobs ESSSA Group-NASA Marshall Space Flight Center, Branch EV44, Huntsville, AL 35812, USA (e-mail: michael.l.goodman@nasa.gov)

[2]Applied Research LLC, 9605 Medical Center Drive-Suite 127E, Rockville, MD 20850, USA

I. INTRODUCTION

There are many flare forecasting models. For an excellent review and comparison of some of them see Barnes et al. (2016). All these models are successful to some degree, but there is a need for better models. We claim the most successful models explicitly or implicitly base their forecasts on various estimates of components of the photospheric current density $\mathbf{J}$, based on observations of the photospheric magnetic field $\mathbf{B}$. However, none of the models we are aware of compute the complete $\mathbf{J}$. We seek to develop a better model based on computing the complete photospheric $\mathbf{J}$. Initial results from this model are presented in this talk. We present a data driven, near photospheric, 3 D, non-force free magnetohydrodynamic (MHD) model that computes time series of the total $\mathbf{J}$, and associated resistive heating rate in each pixel at the photosphere in the neutral line regions (NLRs) of 14 active regions (ARs). The model is driven by time series of $\mathbf{B}$ measured by the Helioseismic & Magnetic Imager (HMI) on the Solar Dynamics Observatory (SDO) satellite. Spurious Doppler periods due to SDO orbital motion are filtered out of the time series of $\mathbf{B}$ in every AR pixel. Errors in $\mathbf{B}$ due to these periods can be significant. For the NLR integrated resistive heating rate Q, the number of occurrences $N(q)$ of values of $Q \geq q$ is the cumulative distribution function (CDF) of Q. For each AR time series it is found to be a scale invariant power law distribution, $N(Q) \propto Q^{-s}$, above an AR dependent threshold value of Q, where S varies little between ARs (§V). For coronal flares, $N(E)$, where E is the total magnetic energy converted into particle energy, is known from observations to have the same form: $N(E) \propto E^{-s}$, s varies between ARs, and the ranges of S and s strongly overlap (§V). This strong similarity between $N(Q)$ and $N(E)$ suggests the same process that powers coronal flares also powers the photospheric Q. Model results also suggest it is plausible that the times of large spikes in Q, several orders of magnitude above background values, are correlated with the subsequent occurrence of M or X flares (§IV). These spikes typically occur a few hours to a few days prior to M or X flares. The spikes correspond to large vertical derivatives of the horizontal magnetic field, suggesting strong heating in horizontal current sheets. The subset of spikes analyzed at the pixel level are found to occur on HMI and granulation scales of 1 arcsec and 12 minutes, suggesting the current sheets are granulation scale. Spikes are found in ARs with and without M or X flares, and outside as well as inside NLRs, but the largest spikes are localized in the NLRs of ARs with M or X flares. Time series from more ARs must be analyzed to statistically determine if this suggested correlation between Q and flares is real.

II. THE MODEL

The model is an MHD model that uses all of the available HMI $\mathbf{B}$ data for a given AR. The model is valid close to the photosphere in that the analytical, semi-empirically determined expression for $\mathbf{B}$ is valid through order z^2, and the $\nabla \cdot \mathbf{B} = 0$ condition is satisfied through order z. The only differential equation in the model is $\nabla \times \mathbf{A} = \mathbf{B}$, for the vector potential $\mathbf{A}$, with the gauge condition $\nabla \cdot \mathbf{A} = 0$. This equation is solved analytically. The electric field $\mathbf{E} \sim -c^{-1}\partial\mathbf{A}/\partial t$. The Ohm's law is $\mathbf{E} + (\mathbf{V} \times \mathbf{B})/c = \eta\mathbf{J}$. $\mathbf{V}$ is the velocity of the plasma. $\eta = 2 \times 10^{-12}$ s is the resistivity. There are no equations for density, temperature, pressure, or momentum. Cartesian coordinates (x, y, z) are used, with z the height above the photosphere. A data determined length scale $L(x, y, t)$ determines $\partial\mathbf{B}/\partial z$ at $z = 0$, allowing the complete $\mathbf{J}(x, y, 0, t)$ to be computed. It is enforcing the $\nabla \cdot \mathbf{B} = 0$ condition that allows $L(x, y, t)$, and hence $\mathbf{J}(x, y, 0, t)$ to be computed. The HMI pixel side length is $\Delta = 0.5''$. Pixel overlap results in a magnetic field resolution $\sim 1''(\sim 725$ km). HMI provides time averaged data with a resolution of 12 minutes. Data from the hmi.sharp_720s_cea data series are used to minimize effects of noise. Every 12 minutes HMI provides a full disk map of $\mathbf{B}$. HMI $\mathbf{B}$ is a function of x, y, and t. Using the CEA (cylindrical equal area) data helps minimize projection error (Sun 2013).

A. Magnetic Field

Let (L_x, L_y) be the (x, y) dimensions of the rectangular region used to enclose the AR modeled. The number of HMI

data points covering this region is $N = (N_x + 1)(N_y + 1)$, where $N_x = L_x/\Delta, N_y = L_y/\Delta$, and N_x, N_y are given by the HMI datasets. For any function $f(x, y, z, t)$, define $f_{,x} = \partial f/\partial x$, and similarly for derivatives with respect to y, z, and t. Let

$$\mathbf{B}(x, y, z, t) = e^{-z/L(x,y,t)} \sum_{n=0}^{N_x} \sum_{m=0}^{N_y} \mathbf{b}_{nm}(t) e^{2\pi i \left(\frac{nx}{L_x} + \frac{my}{L_y}\right)}. \tag{1}$$

Here the $\mathbf{b}_{nm}(t)$ are complex, and $L(x, y, t) = L_0(x, y, t) + zL_1(x, y, t)/L_0$ where L_0 and L_1 are real and determined by the HMI data and the $\nabla \cdot \mathbf{B} = 0$ condition. Equation (1) is valid for sufficiently small z. For $z = 0$, and given the N vectors $\mathbf{B}(x_i, y_i, 0, t_j)$ from the HMI data for each j, Eq. (1) represents N equations for each component of $\mathbf{b}_{nm}(t)$. The time series of $\mathbf{b}_{nm}(t)$is determined by performing an FFT on Eq. (1). The imaginary part of $\mathbf{B}$ must be zero, which is used as a check on the numerical solution for the $\mathbf{b}_{nm}(t)$.

B. The $\nabla \cdot \mathbf{B} = 0$ Condition

Define $\mathbf{B}_0 = \mathbf{B}(x, y, 0, t)$. Take the divergence of the real part of Eq. (1) and set it equal to zero. Solving the resulting equation through order z gives

$$L_0(x, y, t) = \frac{B_{0z}}{B_{0x,x} + B_{0y,y}}, \tag{2}$$

and

$$L_1(x, y, t) = -\frac{L_0}{2B_{0z}} \left(B_{0x} L_{0,x} + B_{0y} L_{0,y}\right). \tag{3}$$

The right hand sides of Eqs. (2) and (3) are evaluated at $z = 0$. Therefore, L_0 and L_1 are completely determined by the HMI data. The resulting expression for $\mathbf{B}$ is valid through order z^2. It is the $\nabla \cdot \mathbf{B} = 0$ condition plus the HMI data that determine the z dependence of the model, which is what allows the complete expressions for J_x and J_y to be computed. Without a determination of the height dependence of $\mathbf{B}$, the components of J_x and J_y that involve $B_{y,z}$ and $B_{x,z}$ at $z = 0$ cannot be computed.

III. REMOVAL OF SPURIOUS DOPPLER PERIODS FROM THE HMI **B** DATA

There is spurious, Doppler shift generated noise in the form of 6, 12, and 24 hour period oscillations in the components of $\mathbf{B}$ for each pixel, corresponding to frequencies of $(4.6296, 2.3148, 1.1574) \times 10^{-5}$ Hz. This noise causes a slow change in $\mathbf{B}$ relative to the granule turnover time since the oscillation periods correspond to 20-60 turnover times. The model removes this noise from the time series of HMI $\mathbf{B}$ for each pixel using an FFT based bandpass filter (S14) that removes frequencies in an interval of length 0.4166×10^{-5} Hz centered on each of the three noise frequencies.[1]

[1] An alternative method for mitigating the spurious Doppler effects is presented in Schuck et al. (2016)

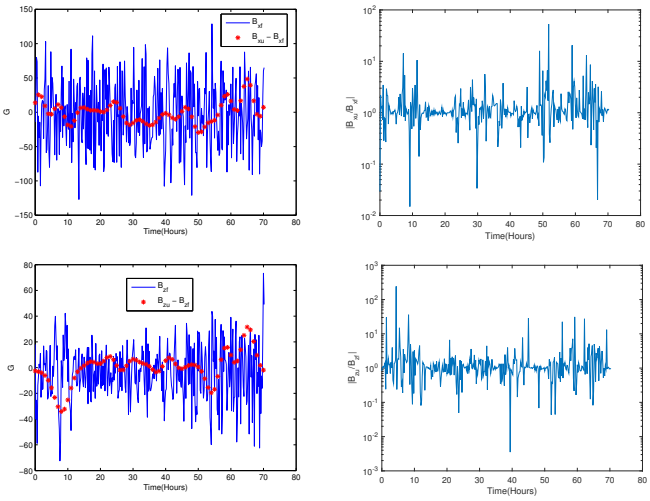

Figure 1. Comparison of Filtered and Un-filtered B_x and B_z in a pixel. B_y, not shown, is similar to B_x.

Denote the filtered and un-filtered time series for B_x as B_{xf} and B_{xu}, and similarly for other quantities. Figure 1 shows the filtered and un-filtered HMI time series of B_x and B_z, the difference between the un-filtered and filtered time series, and the magnitude of their ratio for a randomly selected pixel from the NLR of NOAA AR 1166. This AR is one of the strongly flaring (SF) ARs analyzed here. An SF AR is one with M or X flares. A control AR (C AR) is one with lower class or no flares. The figure shows that the difference between the filtered and un-filtered time series of $\mathbf{B}$ is significant, so Doppler noise can be significant at the single pixel level. Doppler noise can also be significant in quantities that are integrals of pixel level quantities over NLRs. For example, again consider the time series for NOAA AR 1166 used for Fig. 1. Figure 2 shows the results of integrating the filtered and un-filtered pixel level results for $Q = \eta J^2$ and $B^2/8\pi$ over the NLR at each time. The 70 hour long time interval includes 1 X, 2 M, and 9 C flares. For these and subsequent figures, the red, green, and light blue vertical lines and their labels indicate the times and magnitudes of X, M, and C flares. During the 70 hour time interval the number of pixels in the NLR varies across the range of $\sim 3 - 6 \times 10^4$. The figures show that the sum of un-filtered quantities from each pixel causes a large error in the result.

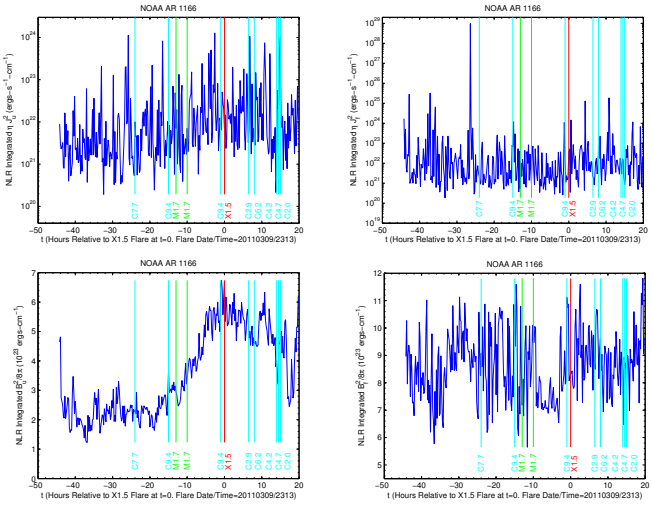

Figure 2. Comparison of filtered and un-filtered NLR integrated $Q = \eta J^2$ and $B^2/8\pi$.

IV. HEATING SPIKES IN SF ARs

In this and the remaining sections of this abstract, unless otherwise indicated, Q stands for the spatial integral of the pixel level Q over the NLR. Figures 3 and 4 show the time series of Q for the 7 SF ARs. The times of the largest spikes in Q relative to the times of M and X flares in these plots indicate it is plausible that these spikes are correlated with the subsequent occurrence of M or X flares, and indicate the need to analyze time series of Q for more ARs to statistically determine if such a correlation exists. The plausibility of a correlation is suggested by the following trends shown in the plots. For AR 1158 the largest spike by a factor ~ 25 occurs $\sim 38 - 68$ hours before the X and M flares. For AR 1166 the largest spike is ~ 3.5 orders of magnitude larger than all others, and occurs 26 hours before the X flare. The next 2 largest spikes occur $\sim 38 - 44$ hours before the X flare. For AR 1261 the 6 largest spikes occur $\sim 18 - 39$ hours before the M flare, and all but one are more than an order of magnitude larger than the 7th largest spike. For AR 1283 the 3 largest spikes occur $\sim 22 - 25$ hours before the X flare, and the 2 largest of these are more than an order of magnitude larger than the 4th largest spike. For ARs 1429 and 1430, which are magnetically coupled in the sense they are merging during the time series, the 9 largest values of Q occur about one day before the two X flares near t=0, but after the X1.1 flare. The meaning of the timing of these spikes for ARs 1429/1430, and for AR 1890 is complicated by the fact that the largest spikes occur between X flares. For AR 1890, for values above background values, which are $\lesssim 10^{23}$ ergs-cm^{-1}-s^{-1}, Q increases from the left towards the first X1.1 flare, attains its largest value between the two X1.1 flares, and tends to decrease after the second X1.1 flare. For AR 2017 the largest spike by an order of magnitude occurs ~ 4 hours before the X flare, and the next 2 largest spikes occur $\sim 90 - 105$ hours before the X flare.

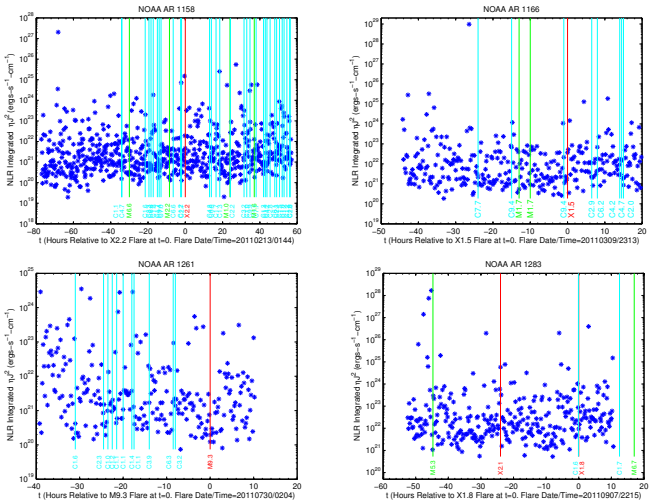

Figure 3. Q for 4 of 7 SF ARs. For AR 1283 the X1.8 and C1.6 flares overlap.

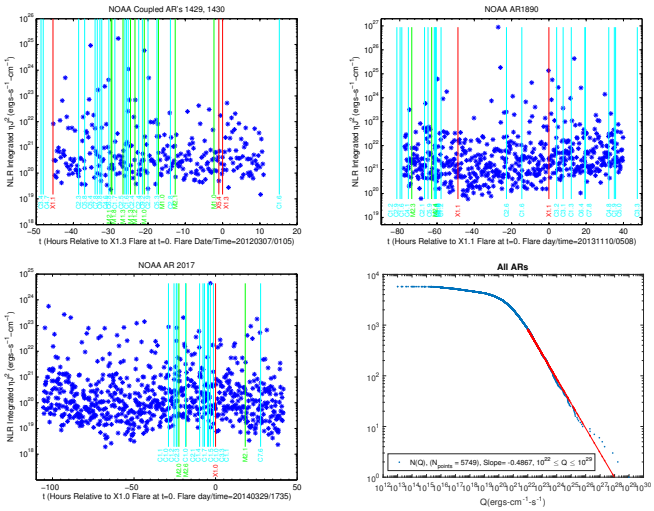

Figure 4. Q for the remaining 3 SF ARs, and $N(Q)$ for all ARs (see §V).

V. THE CDFs OF Q AND FLARES, AND THE POSSIBILITY OF SELF ORGANIZED CRITICALITY (SOC) IN THE PHOTOSPHERE

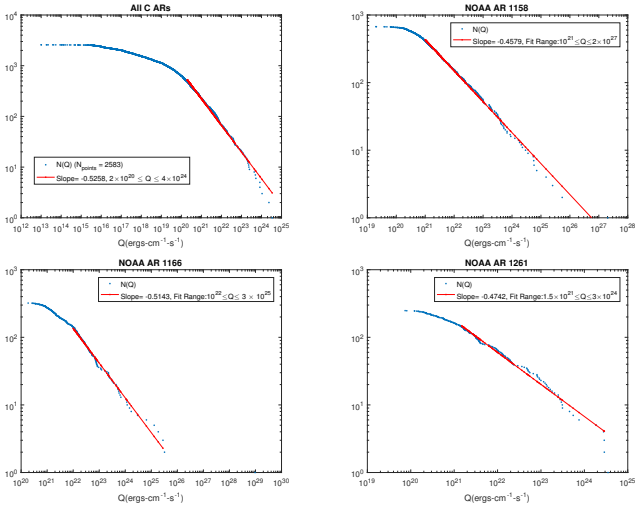

Figure 5. $N(Q)$ for all C ARs, and 3 SF ARs.

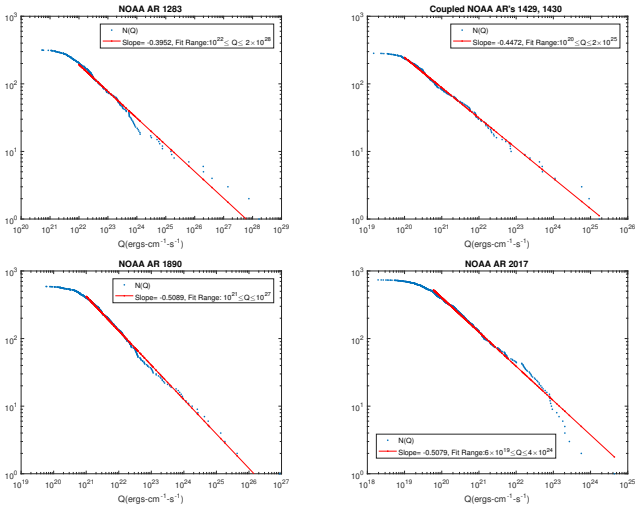

Figure 6. $N(Q)$ for remaining 4 SF ARs.

The CDFs of Q for all ARs, all C ARs, and the 7 individual SF ARs are shown in Figs. 4-6. Log-log plots are used since if $N(Q) = AQ^{-s}$ where A and s are constant over some range of Q, then $\log N(Q) = -s \log Q + \log A$ over this range, which is a line with slope $-s$. CDFs with these properties are called scale invariant power law distributions since the value of s does not depend on any physical scale over this range of Q, so that $N(kQ) = constant \times N(Q)$, where k is any constant. The lines that are fit to the data are generated by the Matlab polyfit function over the range of Q indicated in each figure. In most cases the linear fits are very good over the indicated ranges. In some cases the linear behavior breaks down for $N(Q) \lesssim 10$. Visual inspection suggests that in most cases this breakdown is due to an insufficient number of data points for the higher values of Q, in which case the linear behavior would extend to higher values of Q if longer time series were used to provide better statistics. However, for SF AR 1166 in Fig. 5 there is a data point at $Q = 10^{29}$ ergs-cm^{-1}-s^{-1}, about 3.5 orders of magnitude to the right of the bottom of the linear fit. This suggests that for this AR the scale invariant behavior breaks down for $Q \gtrsim 10^{26}$ ergs-cm^{-1}-s^{-1}.

The figures, including those of $N(Q)$ for the individual C ARs that are not included here, show that the CDFs of the 14 ARs exhibit scale invariant behavior over ranges of Q that extend over $\sim 2 - 2.9$ orders of magnitude for 3 ARs, and over $\sim 3.3 - 6.3$ orders of magnitude for the remaining 11 ARs. The CDFs of all ARs, all SF ARs, and all C ARs show scale invariant behavior over a range of Q that extends over $\sim 4 - 5$ orders of magnitude. This behavior is evidence that whatever process generates Q above an AR dependent threshold value remains the same over the corresponding range of Q. This behavior is a necessary but not sufficient condition for the system, here an AR NLR, to be in an SOC state (Watkins et al. 2016). SOC states arise naturally during the evolution of dynamical systems with extended spatial degrees of freedom, such as the photosphere and corona. They are characterized by long range spatial order, are stable in a narrow range of system parameter values, and exhibit a high degree of chaos and noise (Bak et al. 1987; Tang et al. 1987; Kadanoff 1991; Drazin 1992; Bak 1996; Newman 2005; Watkins et al. 2016), where chaos is deterministic but often indistinguishable from noise due to insufficient resolution. The transition of a system into an SOC state is similar to a phase transition in that the system makes a transition from a state without long range order to one with long range order.

For the SF ARs, s =(0.4472, 0.4579, 0.4708, 0.4742, 0.4858, 0.5101, 0.5143). For the C ARs, s =(0.3351, 0.4080, 0.4303, 0.4356, 0.4459, 0.5148, 0.5385). The range of s is $\sim$ 0.34 − 0.54, with all but one value in the range 0.4 − 0.54. The mean, median, and standard deviation of s for all SF ARs, all C ARs, and all ARs are, respectively, (0.4800, 0.4742, 0.0252), (0.4440, 0.4356, 0.0675), and (0.4620, 0.4643, 0.0524). This shows there is little statistical variation in s among the 14 ARs, so s is largely independent of individual AR properties.

The scale invariant behavior of $N(Q)$, and the range, mean values, and weak dependence of s on AR are similar to the observed properties of the CDF $N(E)$ for coronal flares, where E is the total energy released, defined as the total amount of magnetic energy converted into particle energy. It is observed that above an AR dependent threshold of E, $N(E) = kE^{-\alpha_E}$ where k is an AR dependent constant, and α_E varies little from one AR to another, being largely independent of the differences between ARs such as area, total unsigned magnetic flux, and sunspot distribution (Datlowe et al. 1974; Wheatland 2000, 2010). Observation

based estimates of α_E have been made for over 40 years (Datlow et al. 1974; Hudson 1991; Crosby et al. 1993; Shimizu 1995; Aschwanden & Parnell 2002; Aschwanden 2012, 2013, 2016). For HXR, SXR, and γ ray based constructions of $N(E)$, it is found that $\alpha_E \sim 0.40 - 0.88$, with almost all values in the range of $\sim 0.4 - 0.6$. These observation based values for α_E are consistent with values of α_E predicted by first principles, SOC theories, which give $\alpha_E \sim 0.4 - 0.67$ (Aschwanden & Parnell 2002; Aschwanden 2012, 2013, 2016), and with values of α_E predicted by simulations of the solutions to lattice based avalanche models, which give $\alpha_E \sim 0.40 - 0.57$ (Lu & Hamilton 1991; Lu et al. 1993; Charbonneau et al. 2001; McIntosh et al. 2002; Aschwanden & Parnell 2002; Aschwanden 2012).

Therefore the range of s largely overlaps with the range of α_E, and s and α_E both show relatively little variation with AR. This suggests a common origin of the photospheric $N(Q)$ and the coronal $N(E)$. If they do have a common origin, a question is whether SOC theory can help clarify it. The first application of SOC theory to propose a physical process that gives rise to $N(E)$ is presented in Lu et al. (1991, 1993). There it is proposed that the solar corona is in an SOC state, and that flares consist of a time series of random, spatially distributed avalanche of sub-resolution magnetic reconnection events that trigger one another. If this theory of flares as a coronal process is correct, a question is whether the photosphere is also in an SOC state, and exhibits similar avalanche type flaring events with a similar CDF on smaller energy and spatial scales. The form of $N(Q)$ found here for 14 ARs suggests the answer to this question might be affirmative. The similarity of $N(E)$ and $N(Q)$ discussed above does not prove ARs enter an SOC state when Q exceeds a threshold value, but it is evidence in support of this possibility, and implies it is important to further explore this possibility using time series from more ARs for better statistics.

VI. CONCLUSIONS

The spurious 6, 12, and 24 hour periods in the HMI **B** time series can introduce significant error into **B**, and quantities derived from it.

The CDFs of coronal flares and the photospheric NRL resistive heating events predicted by the model presented here are very similar in that they are both scale invariant, and have power law index ranges that strongly overlap and are largely independent of AR. This suggests that the basic process that drives coronal flares, and the one that drives photospheric heating events are the same process operating on two largely different sets of spatial and temporal scales, and that this process is part of the evolution of the corona and photosphere into SOC states characterized by avalanches in the rate of conversion of magnetic energy to particle energy.

The largest photospheric heating events predicted by the model, corresponding to the largest spikes in Q for ARs with M or X flares are plausibly correlated in time with the subsequent occurrence of M or X flares several hours to several days later, but the sample size of 14 ARs is too small to consider this possibility more than plausible. Analysis of time series from more ARs is necessary to determine if such a correlation exists, and if it is useful for flare forecasting.

REFERENCES

Aschwanden, M.J. 2012, Astron. & Astrophys., 539, A2

Aschwnaden, M.J. 2013, in *Self Organized Criticality Systems*, M.J. Aschwanden (Editor) (Open Academic Press: Berlin, Warsaw), http://www.openacademicpress.de/

Aschwanden, M.J., Crosby, N.B., Dimitropoulou, M., Georgoulis, M.K., Hergarten, S., McAteer, J., Milovanov, A.V., Mineshige, S., Morales, L., Nishizuka, N., Pruessner, G., Sanchez, R., Sharma, A.S., Strugarek, A. & Uritsky, V. 2016, Space Science Reviews, 198, 47

Aschwanden, M.J. & Parnell, C.E. 2002, Astrophys. Journ., 572, 1048

Bak, P. 1996, *How Nature Works* (Springer Science + Business Media New York)

Bak, P., Tang, C. & Wiesenfeld, K. 1987, Phys. Rev. Lett., v. 59, no. 4, p. 381

Barnes, G. & Leka, K.D., Schrijver, C.J., Colak, T., Qahwaji, R., Ashamari, O.W., Yuan, Y., Zhang, J., McAteer, R.T.J., Bloomfield, D.S., Higgins, P.A., Gallagher, P.T., Falconer, D.A., Georgoulis, M.K., Wheatland, M.S., Balch, C., Dunn, T. & Wagner, E.L. 2016, Astrophys. Journ., 829, 89

Charbonneau, P., McIntosh, S.W., Liu, H. & Bogdan, T. 2001, Solar Physics, 203, 321

Crosby, N.B., Aschwanden, M.J. & Dennis, B.R. 1993, Solar Physics, 143, 275

Datlowe, D. W., Elcan, M. J. & Hudson, H. S. 1974, Solar Physics, 39, 155

Drazin, P.G. 1992, *Nonlinear Systems* (Cambridge University Press, Cambridge Texts in Applied Mathematics)

Hudson, H.S. 1991, Solar Physics, 133, 357

Kadanoff, L. 1991, in *Springer Proceedings in Physics*, v. 57, "Evolutionary Trends in the Physical Sciences", Eds.: M. Suzuki and R. Kubo (Springer-Verlag Berlin Heidelberg)

Lu, E.T. & Hamilton, R.J. 1991, Astrophys. Journ., 380, L89

Lu, E.T., Hamilton, R.J., McTiernan, J.M. & Bromund, K.R. 1993, Astrophys. Journ., 412, 841

McIntosh, S.W., Charbonneau, P., Bogdan, T.J., Liu, H. & Norman, J.P. 2002, Phys. Rev. E, 65, 046125

Newman, M.E.J. 2005, Contemporary Physics 46, 323

S14 2014, Final Report for NASA Phase 1 SBIR Contract NNX14CG30P: "A New Class of Flare Prediction Algorithms: A Synthesis of Data, Pattern Recognition Algorithms, and First Principles Magnetohydrodynamics", (Accepted by the NASA Technology Transfer System on December 22, 2014, Case No. GSC-17381-1). The report is available at goo.gl/jQh0YX. Note: The PI name on the report incorrect. The PI is Chiman Kwan. The report was written by the PI and Michael L. Goodman.

Schuck, P.W., Antiochus, S.K., Leka, K.D. & Barnes, G. 2016, Astrophys. Journ., 823, 101

Shimizu, T. 1995, Publications of the Astronomical Society of Japan, 47, 251

Sun, X. 2013, "On the Coordinate System of Space-Weather HMI Active Region Patches (SHARPs): A Technical Note", https://arxiv.org/abs/1309.2392

Tang, C., Wiesenfeld, K., Bak, P., Coppersmith, S. & Littlewood, P. 1987, Phys. Rev. Lett., v. 58, no. 12, p. 1161.

Watkins, N.W., Pruessner, G., Chapman, S.C., Crosby, N.B. & Jensen, H.J. 2016, Space Science Reviews, v. 198, issue 1, pg. 3

Wheatland, M.S. 2000, Astrophys. Journ., 532, 1209

Wheatland, M.S. 2010, Astrophys. Journ., 710, 1324